Spin Coat ZnO Thin Film for Optical and Ethanol Gas Sensing Properties

Sachin T. Bahade*[1], Amrut S. Lanje[1], Satish J. Sharma[2]
*[1]Department of Electronics, Dr. Ambedkar College, Chandrapur, Maharashtra, India
[2]Department of Electronics, R. T. M. Nagpur University, Nagpur, Maharashtra, India

ABSTRACT

In this paper, Zinc oxide (ZnO) thin film synthesized by a simple spin coating sol-gel technique using non-alkoxide Zinc acetate dehydrate, as a precursors. The structural, optical, electrical and gas sensing properties of the film were studied by using XRD, SEM, TEM, FTIR, PL and UV−vis techniques. The X-ray Diffraction (XRD), shows the samples have a Hexagonal wurtzite structure. The Transmission Electron Microscopy (TEM) shows the average particle size is of ~150 nm. Gas sensing performance of synthesized ZnO thin film was tested for ethanol gas at different operating temperatures as well as concentrations.

Keywords: Sol gel, ZnO thin film, Optical, Ethanol Gas sensor, Sensitivity, Reproducibility.

I. INTRODUCTION

Zinc Oxide a multifunctional and sort of II-VI, n-type semiconductor material with broad band gap (3.37 eV) and 60 meV large exciton binding energy at room temperature [1]. ZnO have attracted a lot of interest due to their fascinating features, i.e high surface-to-volume ratio [2], strong carrier confinement [3], enhanced surface modes in their Raman spectra [4], and high transmittance and electrical conductivity [5]. These properties leads to applications in catalysis, gas sensing, and optoelectronics such as light emitting diode, Solar cells and panel displays, [6-8] etc.

Metal oxide Gas sensors are widely using for the detection of toxic and hazardous gases such as CO, NH_3, CH_3OH, H_2S, and LPG etc. and for the prevention of hazardous gas leaks.

The applied synthesis procedures have seen to affect substantially the crystallinity, microstructure and defect structure of the nanocrystallite. Several methods including sol-gel [9-10], thermal evaporation [11], oxalate rout [12] have been utilized to synthesize ZnO. Among these techniques, the sol gel method seems suitable due to its simplicity, easy to add doping materials, promising for mass production and low cost.

The properties of ZnO were found to be dependent on the processing conditions and nature of precursors used. The precursors play an important role in growth, the structure and the morphology as well as optical and electrical characteristics of the material. For optical devices like Solar cells, panel displays applications mainly affected by signal loss and delay, we have to improve the conductivity without affecting the transmission. Similarly, Zinc oxide plays an important role for applications in solar photo-thermal conversion [13, 14]. Due to the limitation of solubility, these ions acts as grain growth inhibitors and remain aggregates at the grain boundaries. In the present work, sol gel synthesized spin coating method employed to obtain ZnO thin film at 500^0C. The properties of Zinc oxide on Crystallographic, Morphological, Optical and Gas sensing characteristics were studied. The obtained results are compared and discussed with several researchers.

II. METHODS AND MATERIAL

A. Synthesis

Nanocrystalline ZnO samples were prepared by a Sol gel rout using Zn precursors taken in the form of acetate. In a typical synthesis process of ZnO, dissolved 8g of Zinc

acetate dehydrate from (Merck, India) in 100 ml ethanol solution (Ethanol+ Water 1:1) and Stirred about 20 min until a transparent sol is produced. Add aqueous Ammonia solution (25% Merck, India) drop wise to the solution under constant stirring and PH of solution was adjusted to a value up to 8. After 24 Hr of aging in the air resulting opal gel were centrifuged and washed with Ethanol at least 5 times to remove ammonia and acetate impurity. The collected gel was dried in furnace over $80^0C/4h$ in the air to remove moisture. Then after crush the sample and sintered at $500^0C/2$ Hr. Finally ash colour nanoparticle were formed [9, 15].

Fabrication of thin film for gas sensor based on the material is done by spin coating method on 10mm x 10 mm glass substrate at 4000 rpm, 30 sec. and dry at 100^0C for 1h, 4 layers and then it was preheated at 200^0C for 2 h and sintered at 500^0C for 2h in air.

B. Characterization techniques

First, the synthesized ZnO thin film were Characterized by X-ray diffraction (XRD) measurements using a Bruker D8 Advance diffractometer with monochromatic CuK_∞ radiation (λ=1.5406 A^0) by recording θ in the range of 20-70^0 in a step of 0.02^0. To study the surface morphology & grain sizes, Scanning Electron microscopy(SEM) JEOL JSM 5600 with Resolution : 3.5 nm, Magnification : x18 to 300,000, Accelerating Voltage : 0.5 to 30 kV and Transmission electron microscopy (TEM) model JEOL/JEM 2100 was employed with acceleration voltage 200kV And 2000X – 1500000X magnification. ImageJ computer program were used to investigate the particle size distributions. Fourier Transform infrared (FT-IR) spectra of the powders were recorded using a Bruker, Germany, Model vertex 70 using the KBr pellet technique in the range 400 to 4000 cm^{-1} with a resolution of 0.5 cm^{-1}. Photoluminescence (PL) studies of prepared samples were carried out using a F-4500 FL spectrometer with 150 W Xenon lamp at room temperature. UV-Vis measurement was recorded using Jasco Spectrophotometer V-770 in a 200-1000 wavelength domain.

Finally, ethanol gas sensing measurement of prepared spin coated thin film were carried out using gas sensing chamber, the change in resistance of sensor were recorded by NI USB 6210 DAQ on PC.

The sensor sensitivity is defined as S = Ra/Rg, Where, Ra is the resistance in ambient air and Rg is the resistance in tested gas. Similarly, ethanol gas response recovery time, reproducibility, stability were also recorded.

III. RESULTS AND DISCUSSION
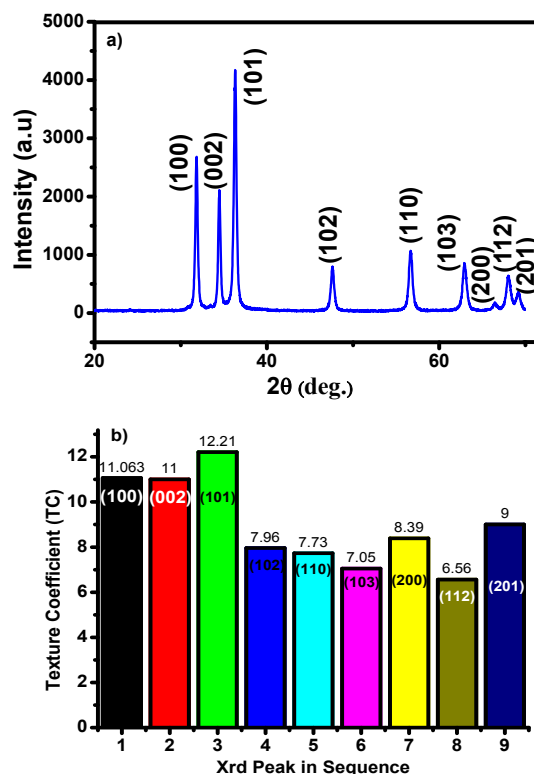
A. Structural Analysis

Figure 1: a) XRD of ZnO at 500^0C
b) Texture Coefficient of ZnO

To study the crystallite size, crystal structure and lattice parameters of ZnO, XRD analysis was used. The X-ray diffraction patterns of ZnO nanoparticles sintered at 500^0C shown in Fig.1.

The peaks were indexed using Powder X software and they are matched with the hexagonal wurtzite structure of ZnO, which are consistent with the values in the standard card (JCPDS -05-0664) with a maximum intensity corresponding to (101) plane. Further it has been observed that lattice parameters a, c and cell volume are calculated using unit cell software program, and as shown in (Table 1). All calculated values are in good agreement with the reported values (JCPDS -05-0664).

Moreover, the texture coefficient (TC) gives information of the maximum preferred orientation along with the diffraction plane, means the increase in the preferred orientation is related with the increase of the number of grains along that plane. $TC_{(hkl)}$ values are calculated from XRD data[16]:

$$TC_{(hkl)} = \frac{I(hkl)/I_0(hkl)}{N^{-1}\Sigma I(hkl)/I_0(hkl)} \text{ ------- (1)}$$

Where, I(hkl) is the measured intensity of X-ray data, $I_0(hkl)$ is the corresponding intensity taking from the JCPDS 05-0664 card and N is the number of diffraction peaks observed in the XRD pattern.

Transmission Coefficient (TC) is one of the important structural parameter to secure the implementation of the prepared materials. The preferred oriented ZnO film is beneficial for improving the electromechanical coupling coefficient of SAW device [17], Optoelectronic and gas sensing application. It is clear from the sample that if TC>1 , this implies that crystal growth occurs in certain preferred orientation. And TC=1, represents randomly oriented crystallites presents. To secure the implementation of the material structural parameter TC is necessary. Figure 1. b) graphically represents preferred orientation of the crystallite.

On the other hand, the average size of the crystalline grains of the sample was calculated using full width half-maximum (FWHM) and Debye-Scherer formula [18] given by :

$$D_{hkl} = \frac{0.9\lambda}{\beta cos\theta} \text{ ----------(2)}$$

Here, D_{hkl} is the crystalline size, λ is the X-ray wave length, β is the (101) full width at half maximum (FWHM) and θ is the angle of diffraction. The estimated size at the most intense crystallographic plane (101) are found to be 26 nm. From the above discussion, it can be concluded that the narrowing or broadening of the XRD peaks of ZnO occurred due to atomic diffusion and lattice strains and not by lattice distortions. The particle size calculated by Scherrer formula for ZnO have been further validated by Transmission Electron Microscopy (TEM).

On the other hand, geometric mismatch between crystalline lattices of thin films and substrate may develop stresses [19], and these stresses can cause microstrains (ζ) in the films. The microstrain values are calculated by following relation [20]:

$$\zeta = (1/sin\theta) [(\lambda/D) - (\beta Cos\theta)] \text{ ------------(3)}$$

Where, β is FWHM of (101) peak and D is the average grain size.

Dislocation is one of the important factor to investigate growth mechanism. It plays an important role in the variation of electrical resistance because the increase in the dislocation density gives rise in disorders, crystal defects in lattice and decreasing crystallinity. Dislocation density (δ) gives information on length of dislocation lines per unit volume (lines/m^2). It can be estimated by following relations [20].
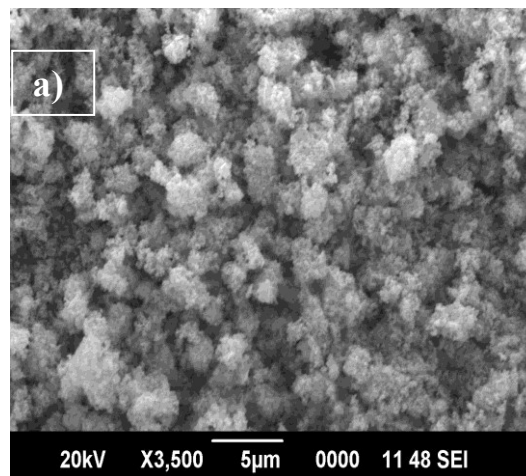
$$\delta = 1/D^2 \text{ --------------(4)}$$

The all calculated values of D, lattice parameter, ζ and δ are given in table 1.

Table 1: The calculated values of the grain size, lattice parameter, microstrain, dislocation density(δ) & Intensity.

	D (nm)	a (Å)	c (Å)	V (Å³)	strain ξ (X 10^{-4})	δ (x10^{14} line/m^2)	Intensity 101
ZnO	26	3.24	5.21	47.51	10.97	14.79	4171

B. Morphological and Compositional Analysis

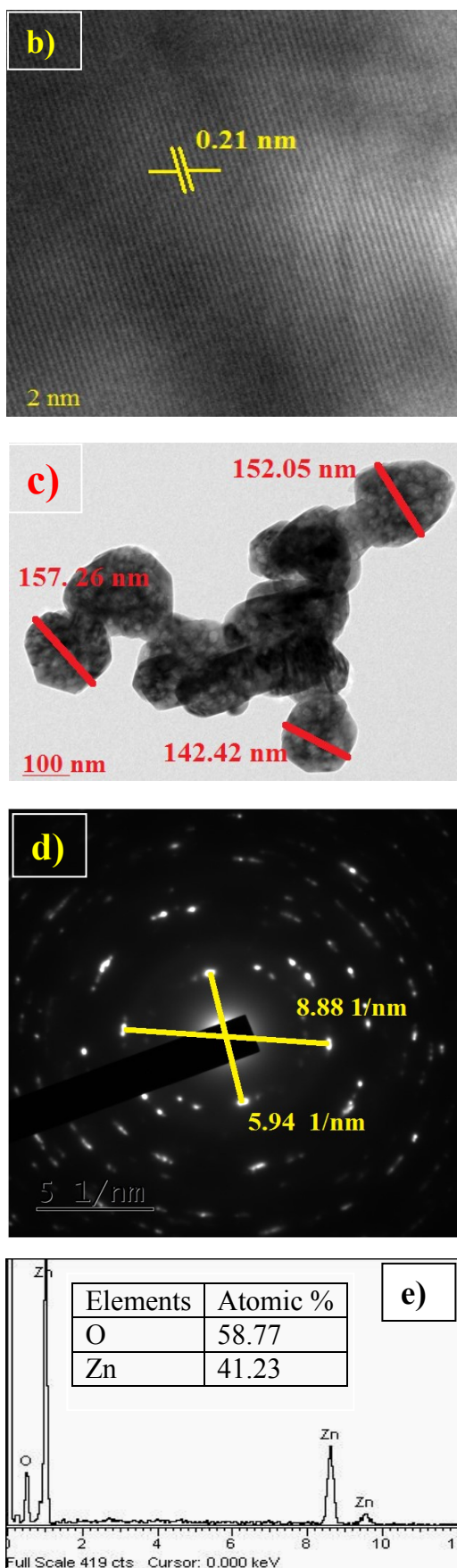| Elements	Atomic %
O	58.77
Zn	41.23

Figure 2: a) SEM b), c), d) TEM images and e) EDAX spectrum of ZnO at 500^0C

Fig.2 a) shows the typical morphology of ZnO nanoparticles. Powder samples were used for SEM analysis. Powder was stick on the sample holder using double sided tape and gold coated with sputter coater. It is seen that SEM image of ZnO microstructure of these powder samples shows the presence of large spherical aggregates of smaller individual nanoparticles with variations in particles size. Due to the large surface and high surface energy of primary nanoparticles. The randomly grown grains gives rise in scattering effect, which reduces the transmittance [21]. The surface state of such oxide nanoparticles influence there optical and electrical properties which are essential to ensure the implementation of the different optoelectronic devices and gas sensors. Fig. 2. b, c, d Shows TEM image of prepared ZnO nanoparticles, showing an average diameter of about 150 nm as well. The particle size obtained from TEM analysis is very higher than the crystalline size calculated from XRD data. There is no clustering or aggregation of nanoparticles in these images which shows good crystalline particles. Fig. 2. e, Shows EDAX spectra with Zn:O ratio as 41.23:58.77, indicates Zn is slightly less than O.
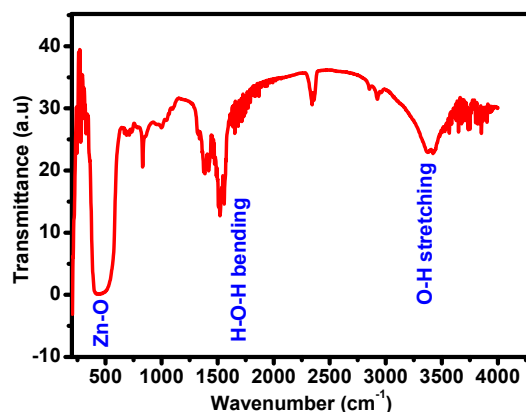
C. FT-IR Analysis

Figure 3: FTIR spectrum of ZnO sample.

FT-IR spectra were recorded in solid phase by using KBr pellets technique in the region of 400-4500cm^{-1}. FT-IR spectra of ZnO nanoparticles prepared at 500^0C are shown in Figure 3. The wavenumber at 500 cm-1 peak corresponds to Zn-O, 1600 peak are due to absorption of water during preparation of IR pellet. The broad bands between 500 and 800 cm-1 were attributed to the vibration of Zn-O bond . In addition to these peaks, peaks at 827, 998, 2343 and 2917 cm^{-1} are due to presence of C-O and C-H vibration modes. The broad peak at 3409 cm^{-1} is pointing to stretching of O-H vibration in the ZnO sample [9]. This confirms the FTIR spectra of the ZnO sample.

D. Uv-vis Analysis

Fig.4 a) shows the absorption coefficient $\alpha(\lambda)$ of ZnO thin film from 200 to 1000 nm range. Samples showing low absorption at higher wavelength and strongest absorption at lower wavelength. The absorption spectra between 200 to 450 nm, shows a maximum around 200 and 300 nm, which indicates the photo-excitation of electrons from the valence band to the conduction band. It is well established that the absorption depends on several factors such as crystalline size, surface roughness, defect density etc. Hence, only the structural study did not reveal significant changes in the morphology of the samples. For that we have to increase of the absorption to increase of the density of the defects and disorder, which are very related to the reduction of crystallite size. Indeed, an increase in dislocation density values and microstrain gives rise to crystal defects and disorders in Zinc oxide lattice [21]. Thus, with more defects, the electronic transitions from the filled valence band to the energy level of defects.

On the other hand, In order to calculate the optical band gap (Eg) we used the Tauc's relation,

$$\alpha h\nu = A'(h\nu - Eg)^n \text{ --------- (5)}$$

Where, α is the absorption coefficient, A is a constant while the exponent n depends on the type of transition (n=2 for indirect allowed, n=1/2 for direct band gap semiconductor). Therefore, the optical band gap is obtained by extrapolation of the linear region of a tauc's plot by plotting $(\alpha h\nu)^2$ vs $h\nu$. The Tauc's plot of ZnO samples are shown in Fig.4 b). The measured band gap Eg was found to be 3.06 eV, which is slightly less to the reported values of bulk ZnO i.e 3.37 eV [1,9]. It can be seen that the band gap values shows decrease tendency in Zinc oxide structures. This can be attributed due to quantum confinement effect [22], reorientation effect [23], microstrain and dislocation density in nanoparticles. Thus, many researchers reported that, with higher level of defects, the electronic transitions occurs from the filled valence band to the energy levels of defects instead of the filled valence band to empty conduction band. These phenomena leads to band tail and shrinkage of the band gag i.e Burstein Moss shift [24]. Fig.4 a), shows the optical Transmittance spectra of ZnO thin film in the wavelength region 200 – 1000 nm. These spectra show that the prepared film exhibit a transparency coefficient lying between (65 to 95 %) in the visible range. The Urbach E_U or band tail energy which characterizes the width of the located state and is associated with microstructural lattice disorder. The Urbach E_U values were obtained from the inverse of the slop of $Ln(\alpha)$ vs $(h\nu)$ Fig. 4 c) of ZnO thin film and calculated value is found to be 0.37 eV.
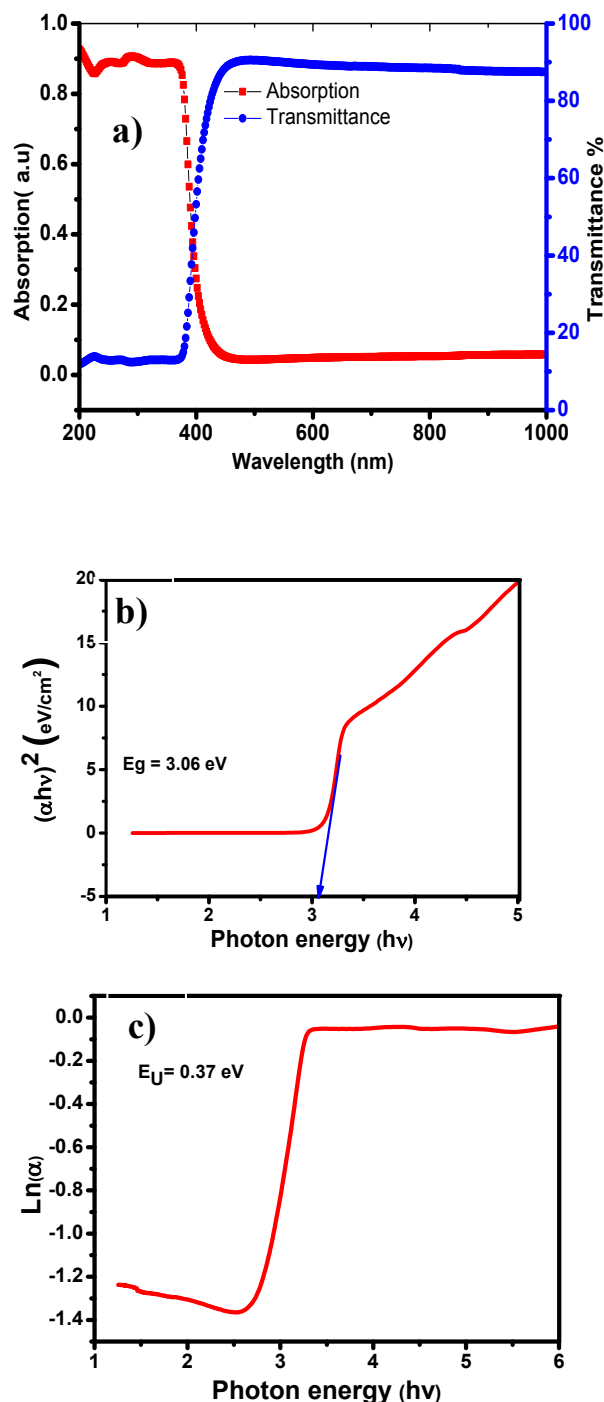

Figure 4: a) Absorption and Transmittance b) Tauc Plot c) Urbach Energy pattern of ZnO thin film.

E. PL Analysis

F. DC Electrical Conductivity

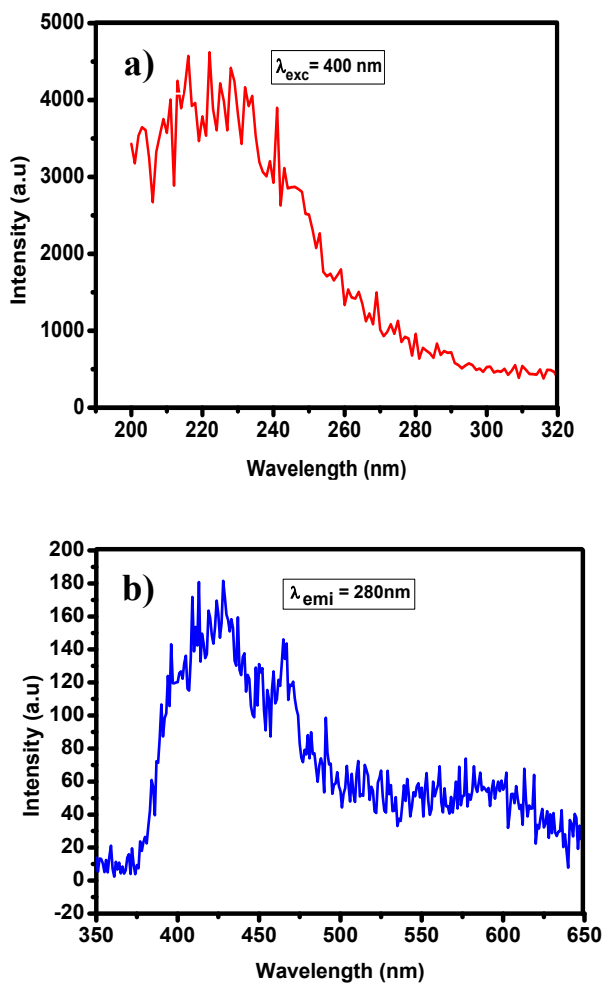**Figure 6:** Conductivity of ZnO thin film

Figure 5 a): PL Emission Spectra of ZnO
b): PL Excitation spectra of ZnO Thin film

PL study can give us significant information on the energy states of impurities and defects, which are useful in study the structural defects in Semiconductors. The room temperature PL behaviour of ZnO thin film was investigated using PL spectrometer. Fig.5 a) contains the photo induced fluorescence spectra for an excitation wavelength 400 nm. It can be seen from the PL spectra, the film exhibit broad emission at 200 to 240 nm and one emission peak at 220 nm. This emission bands presents due to essentially to the presence of point defects, such as oxygen vacancies in ZnO film [25-26].

Fig. 5 b) shows room temperature PL excitation spectra at λemi. = 280nm for ZnO film. The 2 broad excitation bands are observed at 375-475nm at constant emission 280nm. The major peaks are observed of ZnO at 428, 412, 465 nm.
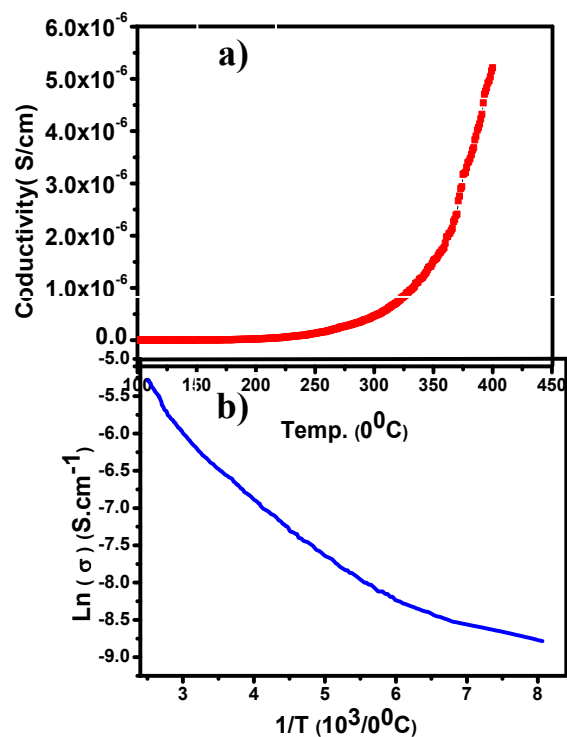
The DC electrical conductivity of ZnO thin film was measured using two probe method in the 100–400 °C temperature range, Fig. 6 a) shows the curve of DC electrical conductivity as a function of temperature. It can be measured that the conductivity of the film increases with temperature, the room temperature dc electrical conductivity is found to be in the range of (0.9 × 10^{-6} S/cm and after heating is increased to 5 × 10^{-6} S/cm at 400 °C). This shows the thermally activated conductivity behavior of ZnO thin film [9]. Which indicates the conductivity increases with the temperature. Fig. 6 b) shows the plot of Ln σ versus 1000/T, From the slope of the Ln σ versus 1000/T curve, activation energy was calculated using the relation [9]:

$$\sigma = \sigma_o \exp(-E_a/kT) \text{ ---------- (6)}$$

where, Ea is the activation energy, k is the Boltzmann constant , T is the temperature, and σ$_o$ is the constant of proportionality. The activation energy of an electrical conduction is found to be (0.58 eV). This activation energy value indicates that the activation of electrons is excited from donor levels to the conduction band, as the temperature is increased. With increasing temperature,

more charge carriers overcome the activation energy barrier and these carriers participate in the electrical conduction [9].

G. Gas sensing performance

Effect Temperature and concentration on gas response:

The Gas sensitivity of Zinc oxide as a function of operating temperature range 200 to 400^0C and Ethanol gas concentration (100 -1500 ppm) is displayed in Fig. 7. Fig. 7 shows sensitivity variation of Zinc oxide sensor at 200 to 400^0C towards 100-1500 ppm of ethanol gas. It is observed that highest sensitivity is achieved under exposure to 1500 ppm of ethanol gas at 350^0C for Zinc Oxide thin film sensor.
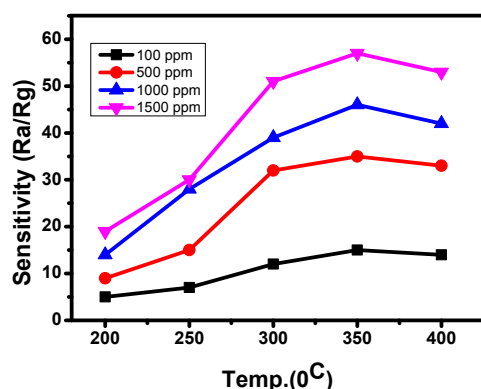

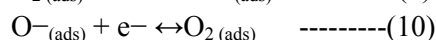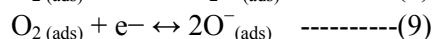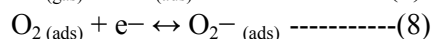**Figure 7**: Ethanol gas sensitivity Pure ZnO

From Fig. 7, it concludes that sensitivity increases with an increase in the operating temperature, reaching maximum value corresponding to 350^0C. However, further increasing the temperature above 350^0C ethanol sensitivity slightly decreases. The optimum sensitivity can be attributed due to thermal energy obtained was high enough to overcome the activation energy barrier of the reaction, while reducing gas sensitivity was due to the difficulty in exothermic gas adsorption [27].

The gas sensing mechanism :

The ZnO thin film based gas sensing mechanism is mainly based on a change in the electrical resistance/carrier concentration due to the oxygen adsorption and reactions of the gases adsorbed on the sensor surface. The oxygen vacancy in ZnO film acts as an electron donor to provide electrons to the conduction

band of ZnO and makes the ZnO film be an n-type semiconductor [28]. In air, the surface of the ZnO film sensor adsorbs some oxygen molecules, this adsorbed oxygen will capture electrons from the conduction band of the ZnO film to become oxygen ions (O^-, O^{2-}, or O_2^-) , mostly O^- is dominant [29]. Consequently, depletion layers in the surface of ZnO thin films causes the carrier concentration to decrease, So the resistance is higher in ambient air.

Also, operating temperature affects the properties of the materials and leading to a difference in the gas sensitivity. It has been observed that, metal oxides mostly sense gases at higher operating temperatures. The operating temperature creates oxygen species on the sensor surface which play an important role in the gas sensing phenomena. The absorption of oxygen depends mainly on the type of materials and their oxidation/reduction reaction with the gas. The following reactions shows how oxygen adsorbed on the sensor surface [30]:

$$O_{2\,(gas)} \leftrightarrow O_{2\,(ads)} \quad \text{----------(7)}$$
$$O_{2\,(ads)} + e- \leftrightarrow O_2-_{\,(ads)} \quad \text{-----------(8)}$$
$$O_{2\,(ads)} + e- \leftrightarrow 2O^-_{\,(ads)} \quad \text{----------(9)}$$
$$O-_{\,(ads)} + e- \leftrightarrow O_{2\,(ads)} \quad \text{---------(10)}$$

Where, O^- is the oxygen adsorption, e^- are electrons. In metal oxide semiconductors, oxygen ions (O^-) work as an acceptor at the surface of the film.

As ethanol gas is introduced, the conductance of the ZnO film will increase and resistance will decrease, due to the exchange of electrons between ionosorbed species and ZnO film i.e releasing the trapped electrons back to the conduction band. The changed in reaction is given by [31]:

$$CH_3CH_2OH_{ads} + 6O_{ads}^- \rightarrow 2CH_2 + 3H_2O + 6e^- \quad \text{----- (11)}$$
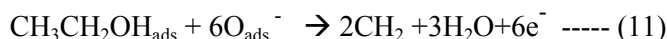
Response and Recovery time:

The response time is, the time taken by the sensor element to achieve 90% of stable output when the gas was introduced. The recovery time is, the time taken by the sensor element to reach 90% of its original value. Fig. 8 shows the response and recovery time of ZnO sensor at 350^0C and 100-1500 ppm ethanol gas. It is observed that when the target gas was inserted in the gas

sensing chamber the resistance of the sensor decrease drastically. However, when air was introduced resistance regains its original value. The time measured between response and recovery is shown details in Fig. 8.
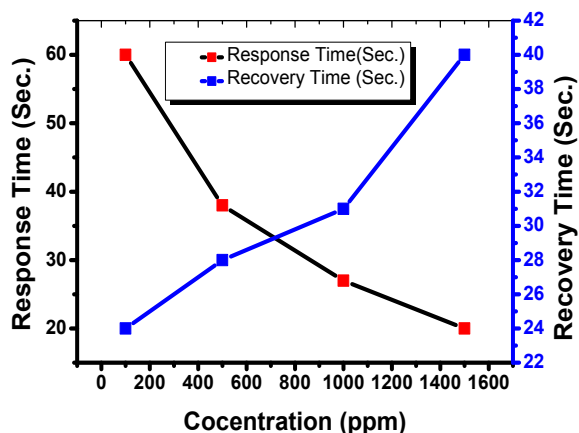

Figure 8: Variation of Response and Recovery Time of ZnO sensor of ethanol concentration.

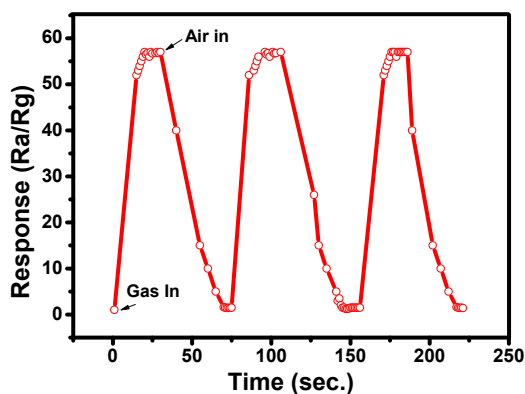*Reproducibility and stability study of ZnO sensor:*

Figure 9 Reproducibility of ZnO Sensor to 1500 ppm of Ethanol gas.

To study the reproducibility of ZnO thin film sensor, the ZnO gas sensing test was repeated three times at 1500 ppm gas concentration and at 350 °C operating temperature, shown in Fig. 9. It is revealed that the gas response of the ZnO sensor towards ethanol is near about constant confirming the reproducibility of the sensor. In order to investigate the stability of the ZnO sensor at 1500 ppm concentration of ethanol gas and at operating temperature of 350 °C, the gas response of the film was measured for 60 days at an interval of 15 days and the result is shown in Fig. 10. From the figure, it is

seen that the gas response dropped initially and after 30 days nearly constant with 3.63% stability. This decrease in the gas sensing response slightly with the number of days can be attributed to the formation of layer oxides/moisture [32]. Thus, it can be concluded that the sensor with high response/selectivity and low response/recovery times based on ZnO thin film can stand as good sensor for detection of ethanol gas.
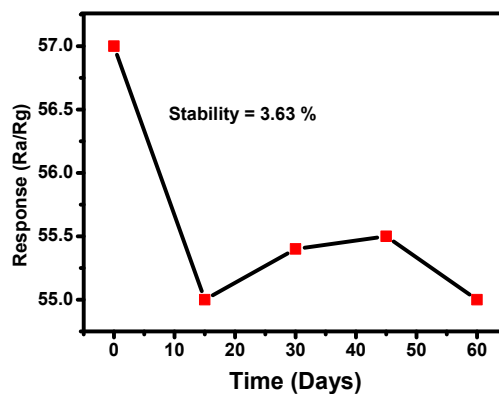

Figure 10: Stability study of ZnO Sensor

IV. CONCLUSION AND OUTLOOK

This paper deals with some structural, optical and Ethanol gas sensing characterization of obtained spin coated thin film by sol gel method at 500^0C.The XRD study shows that the obtained sample has Hexagonal wurtzite structure. SEM images reveal the presence of agglomerates. TEM image confirms that its size greater than with XRD value. Second, PL emission and excitation peaks investigated for photo-catalytic applications. UV-vis has successfully investigated to obtain band gap and band tail value of thin film. Finally, Ethanol gas Sensitivity, Response time, Recovery time, reproducibility, stability was studied by ZnO spin coated thin film sensors. The experimental result indicates that ZnO sensor exhibited highest sensitivity at 350^0C temperature.

V. ACKNOWLEDGEMENT

VI. REFERENCES

[1]. S. I. Inamdar, V. V. Ganbavle, K. Y. Rajpure, Superlattices Microstruct., 76 (2014) 253–263.

[2]. N. S. Baik, G. Sakai, K. Shimane, N. Miura, and N. Yamazoe, (200), Sens. Actuators B, 65 (1-3), 97-100.

[3]. J. H. Lee, C. Reibeiro, T. R. Giraldi, E.Longo and E. R. Leite, (2004), App. Phys. Lett., 84(10), 1745-1747.

[4]. J. Zuo, C. Xu, X. Liu, C. Wang, Y. Hu and Y. Qian , (1994), J. Appl. Phys., 75(3), 1836.

[5]. Marbet, A. Boukhachem, M. Amlouk, T. Manaubi, Journal of Alloys and compounds (2016).

[6]. M. Epifani, J. Arbio, E. Pellicer, E. Comini, P. Siciliano, G. Faglia and J. R. Morante, Cryst. Growth Des. (2008), 8(5), 1774-1778.

[7]. L .H. Qian, K. Wanga, H. T. Fang, Y. Lia, and X .L. Maa, Mater. Chem. Phys. (2007),,103(1), 132-136.

[8]. H. Y. Yang, S. F. Yu, H. K. Liang, S. P. Lau, S. S. Pramana, C. Ferraris, C. W. Cheng, and H .J. Fan (2010), Appl. Mater. Interfaces, 2(4), 1191-1194.

[9]. A. S. Lanje, S. J. Sharma, R. B. Pode, "Functional Nanomaterials Synthesis and Characterization" (2014) LAMBERT Aca. Pub., Germany.

[10]. P. Bhattacharya, P. K. Basu, H. Saha, S.Basu, Sens. Actuators B, 124 (2007) 62-67.

[11]. Jong Soo Lee, M. Saif Islam, Sangtae Kim, Sens. & Actuators B, 126 (2007) 73-77.

[12]. C. Yadav, Richa Srivastava, C. D. Dwivedi, P. Pramanik, Sens. & Actuators B, 131 (2008) 216-222.

[13]. Turgut, E. Sonmez, Superlattices and Microstructures, 69 (2014) 175.

[14]. Elangovan, K. Ramamurthi, Journal of Optoelectronics and Advanced Material, 5 (2003) 45.

[15]. A.M. EI-Sayed, S. M. Yakout, Journal of Research in Nanotechnology, Vol.2016(2016).

[16]. Turgut, E. Sonmez, S. Aydin, R. Dilber, U. Turgut, Ceramics International 40 (2014), 12891.

[17]. Sheng-Yuan Chu, Te-Yi Chen, Walter Water Journal of Crystal Growth, Vol.257, Issues 3-4, Oct. 2003, 280-285.

[18]. D. Cullity, "Elements of X-ray Diffraction" (1978) A.W. Pub. Comp. Inc., Bostan.

[19]. W. D. Nix, Mec., Nadai Medal Lecture, ASME Congress, New York, 2001.

[20]. Amlouk, K. Boubaker, M. Amlouk, M. Bouhafs, J. Alloys Compd. 485 (2009) 887.

[21]. Yakuphanouglu, Y. Caglar, S. Ilican, M. Caglar, Phys. B, 394 (2007) 86.

[22]. T. Takagahara and K. Takeda, Phys. Rev. B, 46 (1992) 15578-15581.

[23]. Turgut, E-F. Keskenler, Se. Aydin, E. Sonmez, S. Dogan, B. Duzgun, M. Ertugrul, Superlattices and Microstructures, 56 (2013) 107.

[24]. Burtein, Phy. Rev. 93 (1954) 632.

[25]. S. Luo, J. Fan, W. Liu, M. Zhang Song, C. Lin, X. Wu and P. K. Chu, (2006) Nanotechnology, 17(6) 1695-1699.

[26]. R. Sánchez, Zeferino la, U. Pal, R. Meléndrez and M. Barboza Flores, Advances in Nano Research, Vol. 1, No. 4 (2013) 193-202.

[27]. J. F. Chang, H. H. Kuo, I, C. Leu and M. H. Hon, Sensors Actuator B Chem.,84 (2002) 258-264.

[28]. C. C. Lin, S. Y. Chem, S. Y. Cheng, H. Y. Lee, Appl. Phy. Lett. 84 (2004) 5040-5042.

[29]. Windischmann, P. Mark, J. Electrochem. Soc. 126 (1979) 627-630.

[30]. K. Arshak, I. Gaidan, Mater. Sci. Eng. B 118 (2005) 44–49.

[31]. T. J. Hsueh, C. Hsu, S. Chang, I. Chen, Sensors. and Actuators B 126 (2007) 473-477.

[32]. P. G. Horrison and A. J. Guest, J. Chem. Soc., Faraday Trans. 83 (1987) 3383.

[33]. S. T. Bahade, A. S. Lanje and S. J. Sharma, IJSRST   Vol. 3 (7) (2017), pp. 567-575.

[34]. S. Lanje, R. S. Ningthoujam, S. J. Sharma and R. B. Pode, Indian Journal of Pure & App. Phy., Vol. 49, 2011, pp. 234-238.

[35]. A. S. Lanje, S. J. Sharma and R. S. Ningthoujam, IJPRET, (2013) Vol. 1(8): 54-63.